JOURNAL OF AIRCRAFT
Vol. 44, No. 3, May–June 2007

Aerodynamic Characteristics of Paradrogue Assembly in an Aerial Refueling System

Kapseong Ro,* Emre Basaran,† and James W. Kamman‡
Western Michigan University, Kalamazoo, Michigan 49008

DOI: 10.2514/1.26489

Unmanned aerial vehicles are now considered an integral part of modern military operations. One of the challenging issues in future unmanned aerial vehicles operations is autonomous aerial refueling, which will raise the current unmanned aerial vehicle mission boundaries set by vehicle endurance and range limitations. Aerial refueling is considered a routine procedure for human operators, but for unmanned aerial vehicle applications, it requires a high level of autonomous technologies based on solid recognition of the overall refueling system design principles. In this paper, the aerodynamic characteristics of a paradrogue assembly in a hose-drogue-probe type of aerial refueling system are investigated through wind-tunnel experiments and computational fluid dynamics simulation analysis. In particular, the drag characteristics of a paradrogue assembly with various component geometric configurations (struts and canopy) are studied. An empirical model based upon a statistical design methodology is constructed, which allows prediction of the drag coefficient of a paradrogue assembly upon these configuration changes.

Nomenclature

α	=	strut angle
$\hat{\alpha}$, $\widehat{GS}$, $\widehat{SA}$	=	normalized value of α, GS, and SA
C_D	=	drag coefficient
D	=	drag
FS	=	fabric spacing
GS	=	gore spacing
p_{node}	=	node pressure
$p*$	=	normalized pressure coefficient
Re	=	Reynolds number
S_{ref}	=	reference area
SA	=	canopy characteristic length
V_∞	=	freestream velocity
ρ_∞	=	freestream density

I. Introduction

WITH the rapid advancement in electronics technologies and their application to aerospace industries, unmanned aerial vehicles (UAVs) have attracted, by far, the most attention since their introduction in the 1800s. One of the important issues in future UAV operations is the extension of range and endurance, which necessitates aerial refueling. For a manned flight, it is regarded as a fairly routine operation, but has never been achieved through a fully autonomous procedure [1]. Although aerial refueling may not be a serious issue for a manned aircraft, it poses a significant problem for future UAV operations. Major government organizations in the United States (such as NASA, the U.S. Air Force, and the U.S. Navy) have already looked into this problem and conducted substantial studies since the early 2000s under the name of the Autonomous Aerial Refueling (AAR) project [2]. Several future research problems are addressed, including the development of a representative dynamic model of the aerial refueling process, which should lead to a model-based control-law design and real-time simulations.

Two common techniques of aerial refueling are the flying boom system and the hose-drogue-probe system. The flying boom is a long pole that is deployed from the rear of a tanker and steered by the tanker crew to dock with a special port on the recipient aircraft. The hose-drogue-probe system involves a tanker aircraft unfolding a long hose, with a drogue at the end containing a high-pressure coupling. This method requires careful flying skills on the receiving vehicle as it attempts to maneuver to plug a probe into the coupling and maintain formation while transferring fuel. One of important tasks in achieving autonomous aerial refueling using the hose-drogue-probe system is to understand the drogue aerodynamics, which will improve the fidelity of dynamic models to be used in control-law synthesis and simulation for autonomous operations. In [1], NASA Dryden Flight Research Center conducted performance flight tests to calculate the aerodynamic drag of an aerial refueling assembly with two drogue assembly types (a higher-drag assembly and a lower-drag assembly) and estimated a constant drag coefficient for the higher-drag assembly for all flight test conditions. It is mentioned that the lower-drag assembly has a highly desirable improvement, because it trails lower behind the tanker.

In general, the hose-drogue-probe refueling system has two possible variants: an integral hose system and a podded hose system. In either system, the drogue is attached to a flexible hose at its narrow end, with a valve where the two meet. It is carried by the tanker aircraft. The receiver plane has a probe, which is a rigid and sometimes jointed arm, placed usually on the side of the aircraft. The tanker flies straight and level, and the drogue is allowed to trail behind and below it. The drogue is not controllable other than by maneuvering the tanker. The receiving aircraft maneuvers into a position to insert its fixed probe into the drogue. When fueling is complete, deceleration of the receiver aircraft disconnects the drogue from the probe. The receptacles of early hose-drogue-probe systems were simply fixed funnels, but it was soon discovered that these systems flew better when holes or longitudinal slits were incorporated. The final evolution was a collapsible drogue, as shown in Fig. 1. The drogue is collapsed when stored and fully expands due to dynamic pressure when deployed. One of the disadvantages of the hose-drogue-probe method is of failing to connect during bad weather or with a damaged aircraft [3]. The success of the refueling depends mostly upon the receiver aircraft pilot's navigation skills. Another disadvantage is that the drogue basket is vulnerable to collapse when the probe approaches the

Presented as Paper 0855 at the 44th AIAA Aerospace Sciences Meeting and Exhibit, Reno, NV, 9–12 January 2006; received 11 July 2006; revision received 8 December 2006; accepted for publication 30 December 2006.

*Assistant Professor, Department of Mechanical and Aeronautical Engineering, College of Engineering and Applied Science. Member AIAA.
†Graduate Student, Department of Mechanical and Aeronautical Engineering, College of Engineering and Applied Science.
‡Associate Professor, Department of Mechanical and Aeronautical Engineering, College of Engineering and Applied Science.

drogue for insertion. If the basket collapses, it gets highly unstable and useless. Considering these facts, understanding the aerodynamic properties of drogue assemblies has vital importance, especially in the application of hose-drogue-probe systems to UAVs.

The main objective of this research is to investigate the aerodynamic characteristics of a drogue assembly using both wind-tunnel experiments and CFD-simulation analysis. This should lead not only to the design criteria for drogue assemblies, but also to improvement of the fidelity of dynamic models for control-system design and numerical simulation. This should advance the aerial refueling automation research. Furthermore, the outcome of this research may be used to establish a design concept for in-flight adjustment of drogue configurations so as to provide an appropriate drag force for a wider range of flight speeds.

II. Description of Paradrogue Assembly

In this paper, a collapsible drogue that consists of a refueling coupling and a paradrogue assembly, as shown in Fig. 1, was studied. The paradrogue is an assembled portion of struts and a drogue canopy. It produces the major portion of the drag, which acts as a reaction force for the probe on the receiver vehicle to engage in the drogue coupling. The aerodynamic force, mainly drag, depends on three geometric characteristics of the paradrogue assembly: strut angle, canopy characteristic length, and canopy gore spacing.

The drogue struts are part of the paradrogue assembly. The actual paradrogue assembly has 36 drogue struts, which are all identical in shape. The strut angle is defined as the angle between the inner strut line and the line that connects the inner and outer mounting holes, as depicted in Fig. 2. The strut angle determines the way the airstreams contact the drogue canopy, similar to an angle of incidence relative to freestream, thus significantly affecting the drag. But it is a fixed angle for a given paradrogue configuration.

The drogue canopy is a ring-shaped component made of nylon fabric, as seen in Fig. 3. Its surface area is characterized by the radial width *SA* from the inner diameter to the outer diameter. The width along with the strut angle determines the amount of billowing of the canopy. The gaps on the canopy are referred to as the gore spacing. Figures 3 and 4 contain an illustration of a paradrogue that is similar to an existing paradrogue. The spacing is determined by partitioning the drogue canopy into six main sections, each taking up 60 deg of arc length of the surface area. In each 60-deg section, there are three smaller divisions that have gores or gaps, and three sections that have strips of fabric (canopy). All of the gores have the same circumferential length, whereas the lengths of the canopy sections vary. Once the size of the gore space is determined, the remaining circumferential length of the 60-deg section is divided by six and called fabric spacing *FS*, that is,

$$FS = (60 - GS \cdot 3)/6 \tag{1}$$

The design of each main section starts with *GS* deg of no fabric followed by *FS* deg of fabric. Then, it has *GS* deg of no fabric followed by $2 \cdot FS$ deg of fabric. The 60-deg section is concluded with *GS* deg of no fabric followed by $3 \cdot FS$ deg of fabric. This 1-2-3 pattern is repeated for each of the remaining five sections, as shown in Fig. 4.

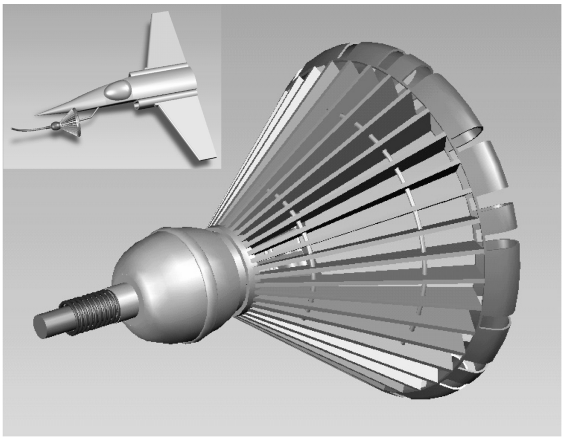

Fig. 1 CAD model of paradrogue assembly.

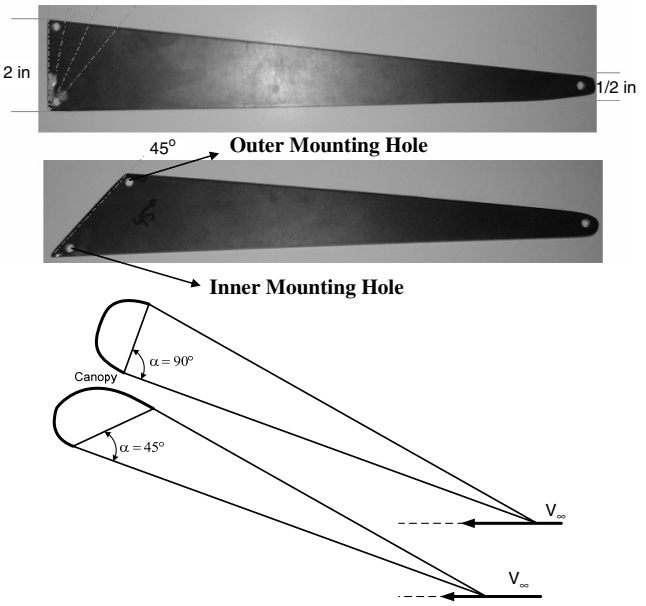

Fig. 2 Strut-angle definition.

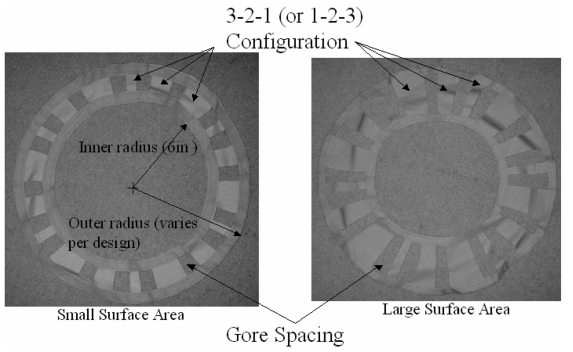

Fig. 3 Canopy characteristic length and gore space definition (wind-tunnel test model).

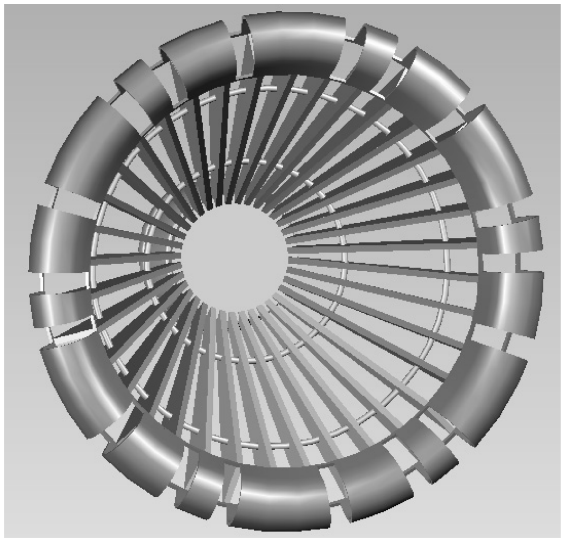

Fig. 4 Gore and fabric space definition (full-scale CAD model).

III. Design of Experiments and Test Description

To study the effect of three geometric characteristics of paradrogue assembly on its total drag, a set of one-half-scale drogue models consisting of different geometric configurations, as described in the previous section, were tested in the advanced-design wind tunnel (ADWT) at Western Michigan University (WMU). The WMU-ADWT is a low-speed, closed-circuit, continuous-flow, single-return, and atmospheric-pressure tunnel with a test section that is 32-in. high, 45-in. wide, 8-ft long, and has a maximum speed of 250 ft/s. A sting-type balance ($\pm 150 \pm 0.01$ lb normal, $\pm 25 \pm 0.01$ lb axial, $\pm 100 \pm 0.01$ lb side, 250-lb-in. pitch, 200-lb-in. roll, and 180-lb-in. yaw) was used to measure the forces and moments on the drogue model. Next, to cross-validate the wind-tunnel test results and to rationalize the aerodynamic effect of those geometric characteristics through flowfield visualizations, CFD-simulation studies were carried out with a widely used commercial CFD software package called FLUENT.

A. Design of Experiments

In this research, an experimental design method called 2^3 full factorial design analysis [4] was implemented to investigate the effect of paradrogue geometric characteristics on total drag. A two-level full factorial design consists of 2^N experiments, where N is the number of factors, each with a high and a low value. In this context, a factor is an experimental variable, and a result is the quantitative measure of the parameter of interest. For this study, three factors (drogue strut angle, drogue canopy characteristic length, and gore spacing), as described in the previous section, were considered. The result was the drag coefficient of the paradrogue. The relevant statistical effects of each factor were found by comparing the results from all of the experiments with the high value of a factor to the results of all of the experiments with the low values. Table 1 shows the design and analysis matrix for the 2^3 full factorial design analysis for the paradrogue assembly wind-tunnel experiment. The $+1$ and -1 are used as normalized values to represent the maximum and minimum values (extremes) to be tested. For example, in test 3, the maximum value is tested for the strut angle and the gore spacing, whereas it has a minimum value for canopy characteristic length.

Running the full set of eight experiments allows estimation of all of the main and interaction effects. As shown in the analysis matrix in Table 1, there are three main effects, three two-factor effects, and one three-factor interaction, all of which appear in the full model, as follows:

$$C_D = \beta_0 + \left(\beta_1 \cdot \hat{\alpha}\right) + \left(\beta_2 \cdot \widehat{SA}\right) + \left(\beta_3 \cdot \widehat{GS}\right) + \left(\beta_{12} \cdot \hat{\alpha} \cdot \widehat{SA}\right) + \left(\beta_{23} \cdot \hat{\alpha} \cdot \widehat{GS}\right) + \left(\beta_{13} \cdot \widehat{SA} \cdot \widehat{GS}\right) + \left(\beta_{123} \cdot \hat{\alpha} \cdot \widehat{SA} \cdot \widehat{GS}\right) \quad (2)$$

where the $\hat{}$ indicates the normalized values of the factors α, GS, and SA. This leads to a statistical estimate of the nondimensional drag coefficient of the paradrogue C_D, where the eight coefficients $\{\beta_0, \beta_1, \beta_2, \beta_3, \beta_{12}, \beta_{23}, \beta_{13}, \beta_{123}\}$ can be statistically determined from the results of the eight tests. For example, the mean effect of strut angle alone on the drag coefficient can be found by

$$\text{first order effect of } (\alpha) = \tfrac{1}{2}\{\text{average}(\alpha+) - \text{average}(\alpha-)\} \quad (3)$$

This first-order effect is the mean of all of the results in which α was a factor minus the average of all of the results in which α was not a factor. Likewise, the first-order effect of GS and SA on the drag coefficient can be found. The second-order effect of α and GS (i.e., $\alpha \cdot GS$) may be found, for example, as follows:

$$\begin{aligned}\text{second-order effect of } (\alpha \cdot GS) &= \tfrac{1}{2}\{\text{mean effect of } \alpha \cdot (GS+) \\ &\quad - \text{mean effect of } \alpha \cdot (GS-)\} = \tfrac{1}{2}\{\text{mean effect of } GS \cdot (\alpha+) \\ &\quad - \text{mean effect of } GS \cdot (\alpha-)\} \end{aligned} \quad (4)$$

The two other second-order effects, $\alpha \cdot SA$ and $GS \cdot SA$, and the third-order effect, $\alpha \cdot GS \cdot SA$, can be found in a similar manner.

The results of factorial design analysis reflect the relative significance of each geometric parameter and their interaction effects on the drag of the paradrogue assembly. This can be qualitatively illustrated by drawing a scree plot or Pareto chart, which is used to justify the relative importance of each of the three main factors and their interactions on the overall paradrogue drag. A factorial analysis of variance (ANOVA) can be performed if a duplicate independent set of experiments is carried out. It provides a quantitative significance of main effects of the independent variable, as well as a significance of interaction effects between independent variables, by computing statistical parameters such as the sum of the squares SS, the mean squares MS, the F-ratios F, and the probabilities P. The true effects can be separated from the effects that are within the experimental error. The lowest probability value from the factorial ANOVA represents the most relevant effect.

B. Wind-Tunnel Tests

A half-scale model was chosen to avoid wind-tunnel wall interaction effects and due to the axial force measurement limitations of the sting balance in the WMU-ADWT. Only eight strut members were used in the test model instead of 36 strut members in the actual paradrogue, due to the complexity in fabricating a half-scale model. The number of struts was not considered to be a major contributing factor to the paradrogue drag. To perform a full 2^3 factorial design analysis, the minimum and maximum values of three geometric parameters of the half-scale model were chosen as follows: the strut angle of 45 deg ($\hat{\alpha} = -1$) and 90 deg ($\hat{\alpha} = +1$), the gore spacing of 5.0 deg ($\widehat{GS} = -1$) and 8.5 deg ($\widehat{GS} = +1$), and the canopy characteristic length of 3.0 in. ($\widehat{SA} = -1$) and 5.5 in. ($\widehat{SA} = +1$), respectively. According to the maximum and minimum values of the canopy characteristic length, the paradrogue component has an outer radius of 9.0 in. (low value) and 11.5 in. (high value). In addition, to test the effect of strut angle, two sets of eight struts (45 and 90 deg) were fabricated using a 1/8-in.-thick metal plate. The strut length is 1 ft for the half-scale model. The paradrogue assembly was held together by a nose cone to take the hose and coupling portion effect

Table 1 Factorial design and analysis matrix

Design matrix				Analysis matrix						
Test runs	Factors			Main effect			Interaction effect			
	$\hat{\alpha}$	$\widehat{SA}$	$\widehat{GS}$	$\hat{\alpha}$	$\widehat{SA}$	$\widehat{GS}$	$\hat{\alpha} \cdot \widehat{SA}$	$\hat{\alpha} \cdot \widehat{GS}$	$\widehat{GS} \cdot \widehat{SA}$	$\hat{\alpha} \cdot \widehat{GS} \cdot \widehat{SA}$
Test 1	+1	+1	+1	+1	+1	+1	+1	+1	+1	+1
Test 2	+1	+1	−1	+1	+1	−1	+1	−1	−1	−1
Test 3	+1	−1	+1	+1	−1	+1	−1	+1	−1	−1
Test 4	+1	−1	−1	+1	−1	−1	−1	−1	+1	+1
Test 5	−1	+1	+1	−1	+1	+1	−1	−1	+1	−1
Test 6	−1	+1	+1	−1	+1	+1	−1	+1	−1	+1
Test 7	−1	−1	+1	−1	−1	+1	+1	−1	−1	+1
Test 8	−1	−1	−1	−1	−1	−1	+1	+1	+1	−1

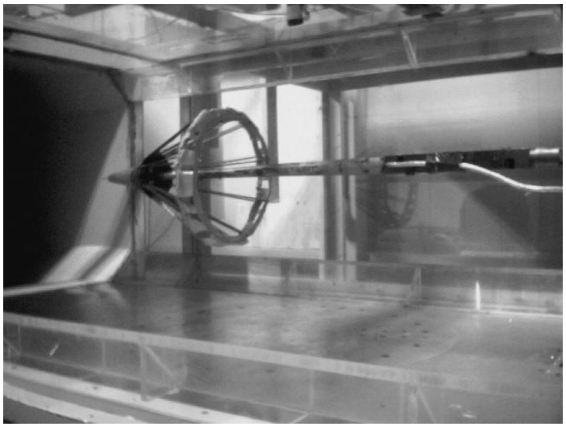

Fig. 5 Wind-tunnel test model.

into account. Figure 5 shows an assembled paradrogue model mounted in the wind tunnel, ready for testing.

A total of 10 wind-tunnel test runs were performed, consisting of two runs without a drogue canopy (strut-only runs) followed by the eight test runs described in the design of experiments (Table 1). All tests were repeated to obtain an independent set of data for statistical analysis associated with experimental errors and the factorial ANOVA. The models were each mounted in sequence and run through the speed range of approximately 30 to 140 ft/s. The three main characteristics measured were the lift, drag, and pitching moment. The drag readings were significant and stable and those for lift and pitching moment were insignificant and thus ignored. The drag coefficient can be computed from the measured drag force as

$$C_D(\alpha, GS, SA) = \frac{D}{1/2\rho_\infty V_\infty^2 S_{\text{ref}}} \tag{5}$$

Note that the reference area used here is a circular area defined by the inner diameter of the paradrogue (i.e., $S_{\text{ref}} = 0.25\pi$ ft^2). The drag coefficient for each model includes the parasite drag from the drogue strut mount. In this study, the drag contribution from the drogue struts-only model (i.e., a model without a drogue canopy) was subtracted from the full model (i.e., a model with a drogue canopy) to isolate the effect of number of drogue struts in the design model.

Figure 6 shows the drag and drag coefficient vs airspeed for eight different paradrogue configurations. A six-digit designation convention is used to identify each data set. The first two digits represent the strut angle, the next two digits represent the canopy characteristic length times 10, and the final two digits represent the gore spacing in degrees times 10. For example, 905585 indicates the paradrogue with a 90-deg strut angle, a 5.5-in. canopy characteristic length, and a 8.5-deg gore spacing. As expected, the 905550 configuration gave the highest drag force, because the higher strut angle results in a larger angle of incidence of inflated canopy relative to freestream. Also, the 5.5-in. canopy characteristic length and 5.0-deg gore spacing gave the largest canopy surface area exposed to freestream in the eight-test set.

The drag coefficient for each configuration is reasonably constant in the high-speed regime (greater than 80 ft/s), in contrast to the lower-speed regime of less than 80 ft/s. This may be due to the presence of struts in front of the canopy that would not allow the fully developed flow to reach the canopy area at low speeds. For this reason, only high-speed regime data points were used for the full factorial analysis. The averages of the drag coefficients in the higher-speed regime were used to calculate the effects for each of the independent variables or factors, and the interactions among them, in the factorial design. The test results are presented in Table 2 (columns labeled WT-1 and WT-2). Finally, the empirical drag coefficient model of the paradrogue assembly based on the full factorial design as expressed in Eq. (2) is given by

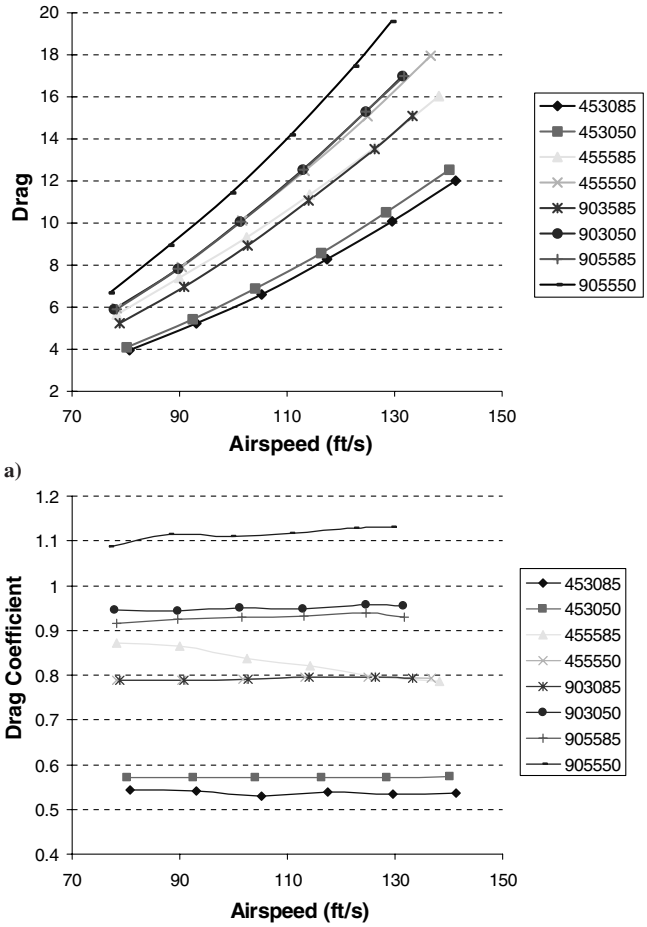

Fig. 6 Wind-tunnel test a) drag comparison and b) drag coefficient comparison.

$$\begin{aligned} C_D = {} & 0.83068 + (0.11872 \cdot \hat{\alpha}) + (0.11555 \cdot \widehat{SA}) \\ & - (0.06195 \cdot \widehat{GS}) - (0.03928 \cdot \hat{\alpha} \cdot \widehat{SA}) - (0.02635 \cdot \hat{\alpha} \cdot \widehat{SA}) \\ & - (0.01310 \cdot \widehat{SA} \cdot \widehat{GS}) + (0.00431 \cdot \hat{\alpha} \cdot \widehat{SA} \cdot \widehat{GS}) \end{aligned} \tag{6}$$

Note again that each factor takes a value between -1 to $+1$. So, for example, the value for the strut angle of 60 deg in Eq. (6) is -0.3333.

C. CFD-Simulation Tests

To cross-validate the wind-tunnel test results, CFD-simulation tests were carried out using a popular commercial CFD software package called FLUENT. To generate the numerical grid model of the paradrogue assembly for CFD analysis, a three-dimensional solid modeling software and a CFD preprocessor called GAMBIT were used. Figure 7 shows the computer generated three-dimensional models of half-scale paradrogue assemblies used for CFD analysis,

Table 2 Experimental drag values for factorial design analysis

Drogue model	Drag coefficient, C_D			
	WT-1	WT-2	CFD	% difference
905585	0.9281	0.9289	0.8709	6.2035
905550	1.1144	1.1312	1.0815	3.6783
903085	0.7922	0.7951	0.6557	17.3817
903050	0.9497	0.9555	0.8073	15.2529
455585	0.8298	0.7977	0.6168	24.2027
455550	0.9235	0.9162	0.7351	20.0848
453085	0.5371	0.5480	0.4744	12.5610
453050	0.5720	0.5786	0.5396	6.2054

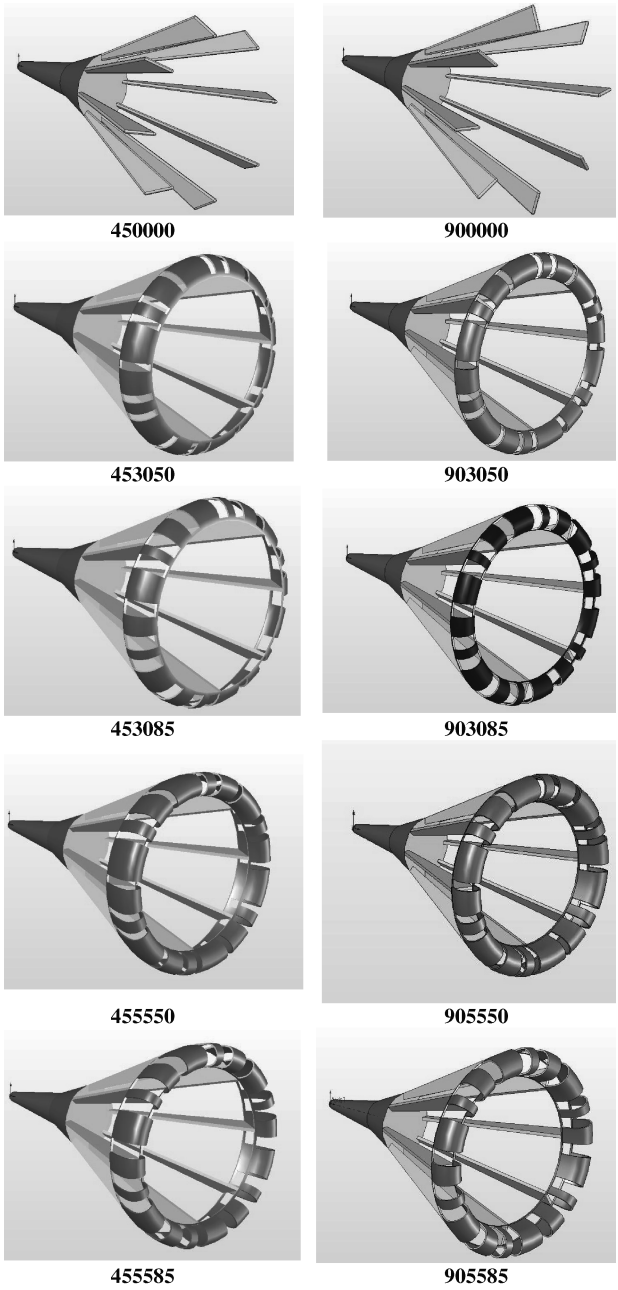

Fig. 7 Solid models for paradrogue with 45XXXX and 90XXXX configuration.

similar to those 10 configurations being tested in the wind-tunnel experiments.

One of the most difficult tasks in generating a computer model of a paradrogue assembly is to represent the drogue canopy as a solid surface, because it is made of flexible nylon fabric and its profile shape depends on many parameters such as the airspeed, strut angle, gore spacing, and the fabric material properties (including permeability). The effects of these variables on the profile shape are very difficult to understand and to correctly reflect in the solid modeling process, and so the profile images observed during the wind-tunnel tests were used to create the CFD model in this study. Based on observations made during the wind-tunnel tests, four different drogue profiles were used in the CFD analysis for the models of 4530XX, 4555XX, 9030XX, and 9055XX, respectively.

To isolate the effect of the strut elements on the total drag of the paradrogue assembly, two strut-only models (each with eight struts) were created. For CFD analysis of these two models, numerical grid models representing one-sixth of the full cylinder with periodic boundary conditions were used to reduce overall computation time.

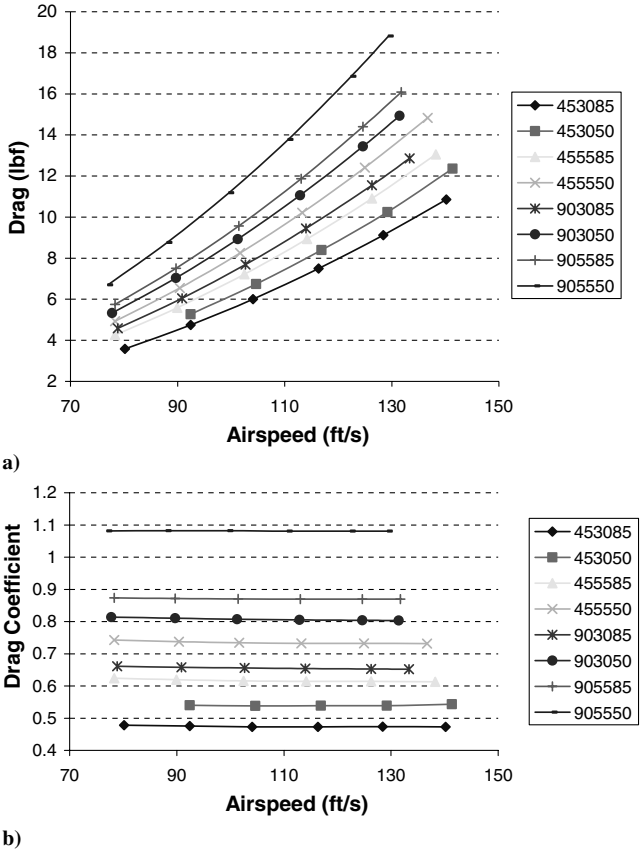

Fig. 8 CFD a) drag comparison and b) drag coefficient comparison.

On the other hand, for the entire paradrogue assembly model with drogue canopy, periodic boundary conditions could not be imposed, due to model asymmetry associated with canopy gore spacing. Instead, the entire cylindrical volume was used to create the computational grid model with the help of the sizing function in GAMBIT. For the entire single-volume mesh model, two different boundary conditions were prescribed, as given in the FLUENT solver: the velocity inlet and the pressure outlet. An unstructured, tetrahedral mesh (T-grid) is generated for the entire volume. The size of the fluid volume was kept the same for all cases. Different mesh sizes were tested and the mesh density around the paradrogue assembly was adjusted to get grid-independent results (achieved at 2,000,000–2,300,000 cells). On the other hand, as mentioned earlier, periodic conditions were imposed and one-sixth of the fluid volume was used for the strut-only model. Different mesh sizes were also tested, and grid independent results were achieved at 300,000–330,000 cells.

The CFD-simulation analysis was carried out based upon incompressible, steady, three-dimensional viscous flow assumptions. The effects of turbulence were modeled using the realizable $k-\varepsilon$ turbulence model. The effect of gravity was neglected. The first 500 iterations were executed with the first-order discretization schemes and then switched to higher-order discretization schemes. Results converged after 1500 iterations, with a convergence criterion of 10^{-5}. The range of Reynolds Re number for the wind-tunnel test runs was from 400,000 to 800,000. Figure 8 shows the drag and drag coefficient vs airspeed for the same eight different types of paradrogue configurations used in the wind-tunnel tests. The average drag coefficients for each model are also presented in Table 2 (CFD column).

IV. Results Analysis and Validation

The major goal of factorial design is to identify key factors that influence the drag of the paradrogue. The results of factorial design of the wind-tunnel tests can be qualitatively represented by a Pareto

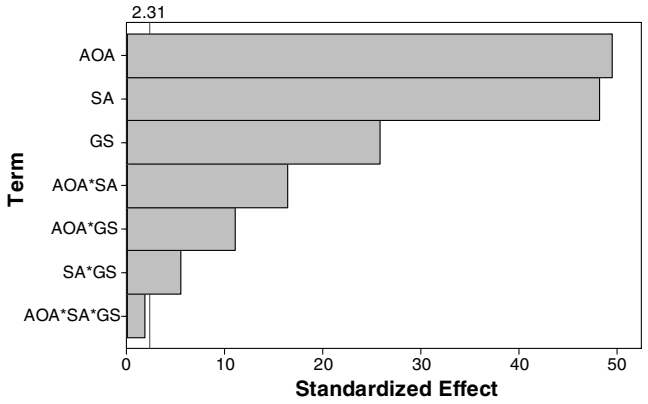

Fig. 9 Pareto chart for wind-tunnel test results.

chart, as shown in Fig. 9. It displays the absolute value of each effect of the three main factors and interaction among them, thus comparing the relative importance in the overall paradrogue drag. The value of 2.31 on the Pareto chart is a reference value computed from the statistical analysis of experimental errors (95% confidence level of the normal probability distribution) from the two sets of wind-tunnel tests. It may be used to determine the importance of each effect. For example, the three-way interaction effect is falling below the experimental error ranges and so its effect on the total drag can be neglected. From the Pareto plot in Fig. 9, it can be concluded that the strut angle and the canopy characteristic length are the two most important factors, with almost equal magnitude in determining the paradrogue drag. The two-way interaction effects are also substantial.

To validate the empirical formulas described by Eq. (6), six additional paradrogue models within the limits of independent variables were fabricated and tested in the wind tunnel, and their drag coefficients were calculated in the same manner as the factorial design analysis. The results are presented in Table 3, along with the predicted drag coefficient using Eqs. (6). Note that the model 60-375-75 represents the canopy characteristic length of 3.75 in. and the gore spacing of 7.5 deg. The predicted value from Eq. (6), that is, the factorial design model based on the wind-tunnel tests, shows good agreement with the validation run results (less than 6.4% difference in 753050).

The numerical solutions obtained from the CFD analysis enable the graphical visualization of the flowfield properties, from which the effect of important design parameters on the paradrogue drag coefficient may be understood. By observing velocity and pressure distributions represented in terms of color contour plots, important flowfield characteristics around the paradrogue and their changes with those geometric variables can be understood. Figure 10 shows the definition of the midsection plane and the region of interest, and Fig. 11 shows the contour plots of dimensionless pressure p^*, defined as the ratio of the node-pressure values to the dynamic pressure:

$$p^* = \frac{p_{\text{node}}}{(1/2)\rho_\infty V_\infty^2} \tag{7}$$

The velocity magnitude contours are shown in Figs. 12a and 12b, and the velocity vector plots are shown in Figs. 12c and 12d, with a detailed view of section B in Figs. 12e and 12f. From these contour

Table 3 Validation run results

Model	WT test	Predict-WT	% difference
60-375-75	0.7494	0.7190	3.9981%
60-475-60	0.8610	0.8536	0.7913%
753050	0.8840	0.8212	6.4490%
75-375-60	0.8550	0.8541	0.3005%
755550	1.1251	1.0481	6.2114%
75-475-60	0.9473	0.9405	0.7263%

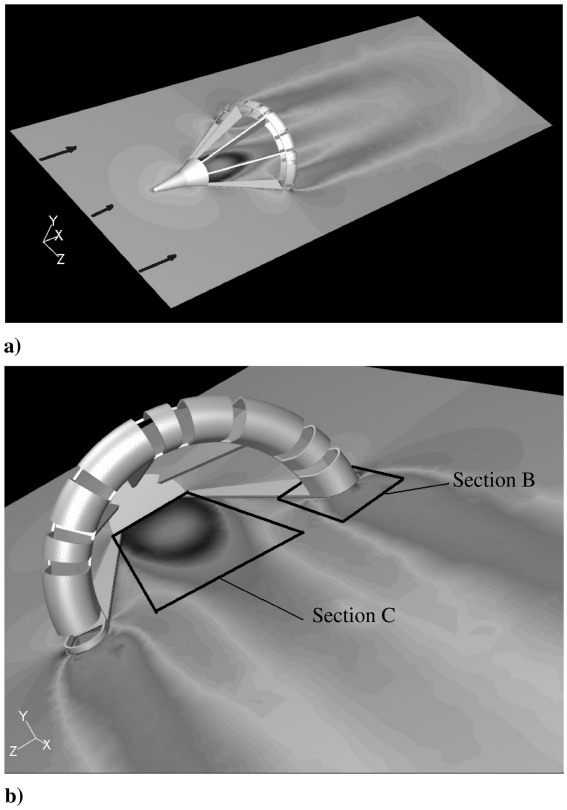

a)

b)

Fig. 10 Velocity magnitude contours a) of the midsection and b) of sections B and C.

plots, it can be observed that the highest-pressure regions are at the tip of the cone (where the top angle of the cone changes) and inside the paradrogue canopies. It is clear that a 90-deg strut-angle configuration has larger pressure gradients at the tips of the struts than the 45-deg configuration. In both configurations, the canopy behaves as a bluff body, and the effects of the strut angle and the fabric size can be observed. The velocity vectors in Figs. 12e and 12f indicate circulations in the inner surface of the canopy. The dimensionless surface-pressure contours shown in Fig. 13 illustrate the high-pressure region inside the canopy.

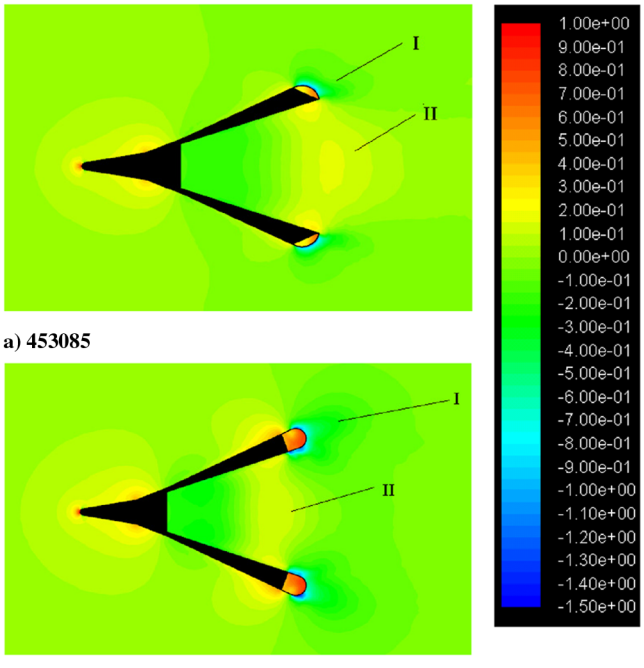

a) 453085

b) 905550

Fig. 11 Pressure (p^*) contour.

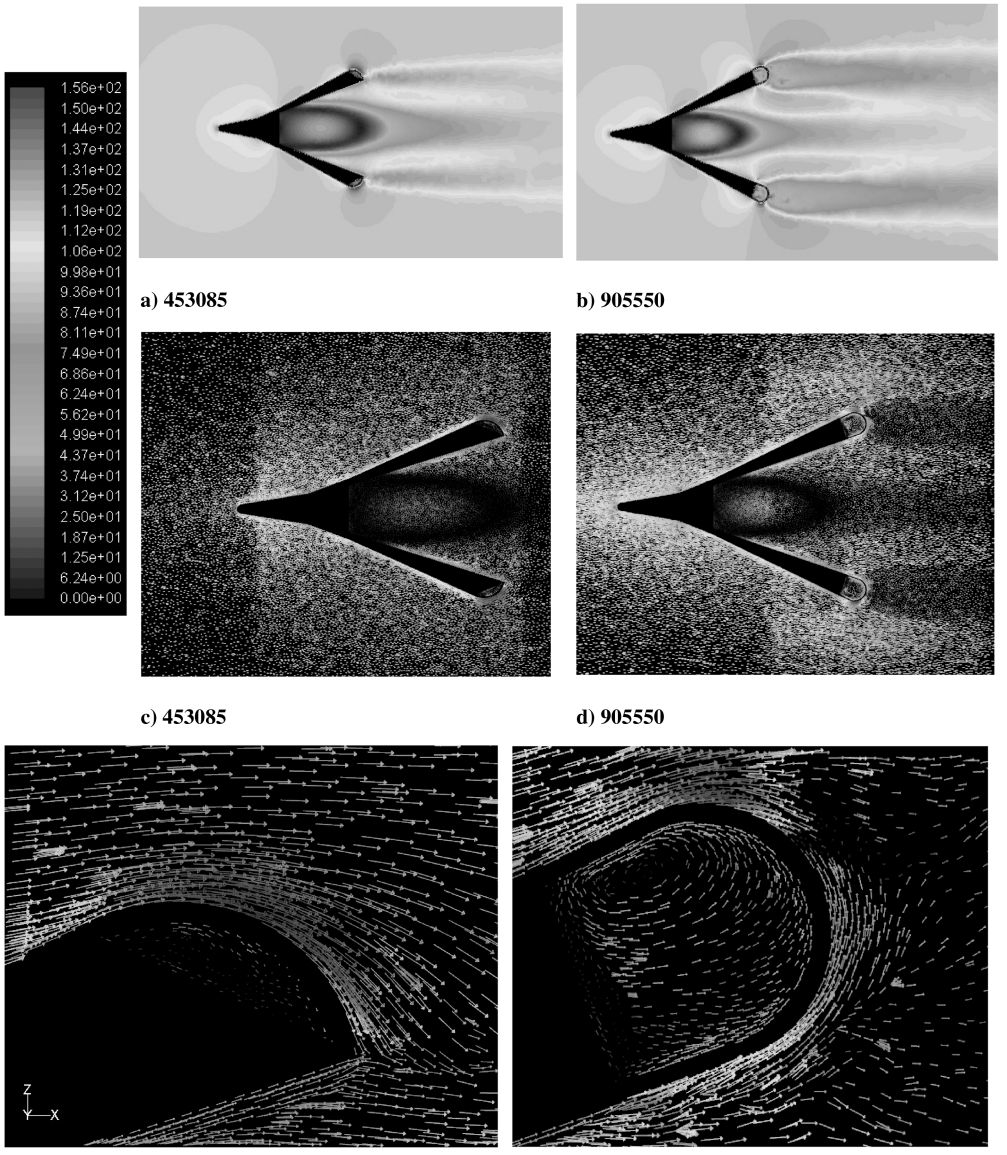

a) 453085 b) 905550

c) 453085 d) 905550

e) 453085 f) 905550

Fig. 12 Velocity magnitude and vector plot.

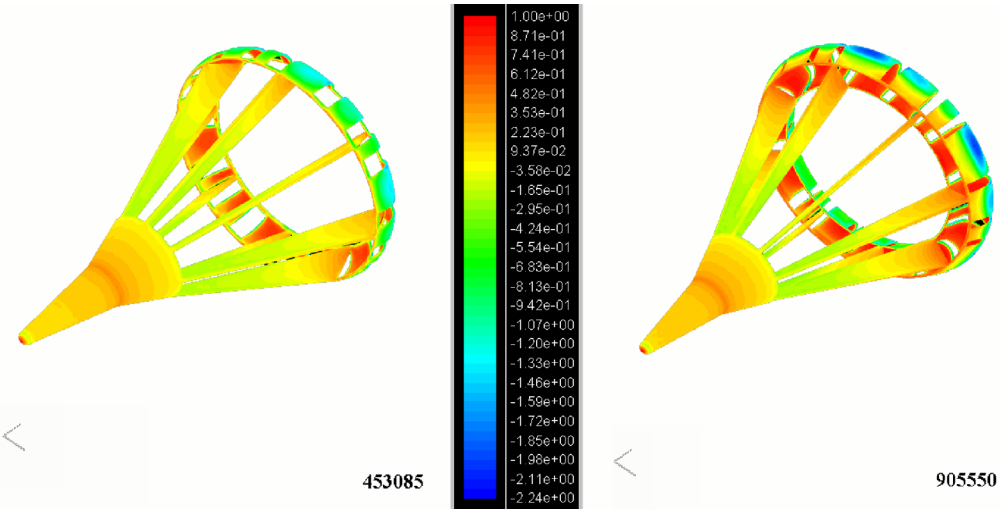

Fig. 13 Surface pressure contours p^* of 453085 and 905550.

At the outer surface of the 90 and 45-deg canopy configurations, different flow patterns are apparent. For the 45-deg configuration, the p^* values are not as low as the 90-deg configuration, because the strut angle of the 45-deg configuration is more streamlined compared with the 90-deg configuration. Furthermore, there is no separation behind the 45-deg configuration, contrary to the 90-deg configuration in which the separation is clearly visible. Flow separation behind the cone can be observed for both configurations in Figs. 12c and 12d, which is also evident from the dimensionless pressure contours at the midsection shown in Fig. 11 as well as the surface p^* contours in Fig. 13. There exists good agreement between these plots, that is, circulating vectors and low-pressure values in the separated flow region behind the cone.

The paradrogue configuration also affects the pressure gradient in the wake regions I and II. The p^* pattern behind the drogue canopy (region I) has smaller values in the 90-deg configuration. It is also interesting to observe that the paradrogue configuration alters the region of low pressure that is related with separation (region II). For example, for the 45-deg configuration, it is behind the drogue canopy, whereas it has moved in front of the canopy for the 90-deg configuration.

As in the wind-tunnel test results, the CFD-simulation tests predicted the highest drag coefficient for 905550 and the lowest drag coefficient for 453085, with a 6.2% difference, as shown in Table 2. It is also interesting to observe that both the wind-tunnel and CFD tests exhibit lower drag values for the 8.5-deg gore-spacing configuration than for the 5-deg configuration for the same strut angle and canopy area configuration. This physically makes sense because the higher gore spacing indicates the less projected area normal to the freestream flow direction. On the other hand, there are some discrepancies in the other cases, such as a 24.2% difference in the 455585 configuration. These discrepancies are thought to arise mainly from the drogue canopy profiles used for CFD-simulation tests, which were based on the visual observations during the wind-tunnel tests. Note that the average value of the WT-1 and WT-2 wind-tunnel values was used to calculate the percent differences.

V. Conclusions

The steady-state aerodynamic characteristics of a paradrogue assembly were investigated through wind-tunnel experiments and computational fluid dynamic analysis. The drag characteristics were studied as a function of geometric parameters of the paradrogue assembly, and an empirical model was obtained based on a statistical design that allows prediction of the drag coefficient of different models within the defined boundaries. Good agreement was found between the CFD and the wind-tunnel test results for the highest and the lowest drag configuration, although CFD-simulation results somewhat underpredict the drag coefficient. The CFD results are highly dependent on the canopy profile images that were taken during the wind-tunnel experiment, and so the discrepancies may be minimized if the drogue canopy profile is more precisely represented. Although the drogue canopy profile is thought to be the primary source for the discrepancies between the wind-tunnel and CFD results, several other factors may contribute, including the CFD analysis inaccurately reproducing the wake of the paradrogue or misrepresenting the flow separation, especially along the rear portion of the paradrogue nose section. This requires some further investigation through additional CFD runs to identify the sources of the discrepancies, and it is beyond the scope of the current study.

Nevertheless, the prediction model based on the wind-tunnel test results produced excellent agreement with the wind-tunnel validation run results, as verified in the validation run cases. From these results, the drag coefficient of a paradrogue assembly can be predicted based on changes of its component geometry, thereby providing a guide for the future paradrogue design. However, it should be noted that the prediction model is based on the scaled model, and one must be cautious when extrapolating for either a smaller or a larger paradrogue, because the factorial design analysis may not guarantee the correct results beyond its predefined range of analysis.

Because the present work is based on a paradrogue with 8 strut members instead of the full 36 struts, future work may be necessary to investigate the full strut model. Conducting a wind-tunnel experiment with the full 36 struts in the actual paradrogue model may be quite involved and expensive, especially incorporating the effect of geometric changes, as in the design experiment described in this paper. Alternatively, computational fluid dynamic simulation tests would predict with reasonable accuracy, as discovered in this study.

Acknowledgments

The first author expresses special gratitude to Hilda Vivas and Mike Booms, senior aeronautical engineering undergraduate students at Western Michigan University, for their efforts in fabricating the test models and running wind-tunnel experiments.

References

[1] Vachon, M. M., Ray, R. J., and Calianno, C., "Calculated Drag of an Aerial Refueling Assembly Through Airplane Performance Analysis," NASA TM-2004-212043, 2004.

[2] Hansen, J. L., Murray, J. E., and Campos, N. V., "The NASA Dryden AAR Project: A Flight Test Approach to an Aerial Refueling System," *AIAA Atmospheric Flight Mechanics Conference and Exhibit*, AIAA, Reston, VA, 2004, pp. 103–115.

[3] Smith, R. K., "Seventy Five Years of Inflight Refueling, Highlights, 1923–1998," *Air Force History and Museum Program*, U.S. Government Printing Office, Washington, D.C., 1998.

[4] Box, G. E. P., Hunter, W. G., and Hunter, J. S., *Statistics for Experimenters: An Introduction to Design, Data Analysis, and Model Building*, Wiley, New York, 1978.